

Probing sterile neutrino freeze-in at stronger coupling

Niko Koivunen,^a Oleg Lebedev,^b Martti Raidal^a

^a*Laboratory of High Energy and Computational Physics, NICPB, Rävåla pst. 10, 10143 Tallinn, Estonia*

^b*Department of Physics and Helsinki Institute of Physics, University of Helsinki, Gustaf Hällströmin katu 2, FI-00014 University of Helsinki, Finland*

E-mail: niko.koivunen@kbfi.ee

ABSTRACT: The regime of dark matter (DM) freeze-in at stronger coupling interpolates between freeze-in and freeze-out. It relies on Boltzmann-suppressed dark matter production, implying that the Standard Model bath temperature never exceeds the dark matter mass. In this work, we study this regime in the context of sterile neutrino dark matter, which can be sufficiently long-lived for a tiny sterile-active mixing. The sterile neutrino is assumed to couple to a real singlet scalar, providing for a thermal production mechanism of the former. We find that DM mass can range from GeV to tens of TeV consistently with all the constraints. The most interesting aspect of the consequent freeze-in phenomenology is that the sterile neutrino dark matter can be probed efficiently by both direct detection experiments and invisible Higgs decay at the LHC.

Contents

1	Introduction	1
2	The model	2
3	Boltzmann-suppressed dark matter production	3
3.1	Heavy dark matter	4
3.1.1	The Boltzmann equation	4
3.1.2	Relic abundance of dark matter and constraints	5
3.2	Light dark matter	8
3.3	Beyond the instant reheating approximation	10
4	Conclusion	11
A	Appendix	12

1 Introduction

Understanding the nature of dark matter (DM) remains one of the main challenges of modern physics. If it is due to a new particle, the latter has to interact sufficiently weakly with matter and be stable or almost stable. The sterile neutrino is an attractive dark matter candidate [1, 2] as long as its mixing with the active neutrinos is tiny, making it long-lived on the cosmological scales [3]. The corresponding constraint as a function of its mass can be found in Ref. [4]. In this work, we call a sterile (or right-handed) neutrino a fermion with the corresponding quantum numbers, i.e. neutral under the Standard Model (SM) gauge symmetries. It is not necessarily responsible for the active neutrino masses since this can be accomplished by heavier, unstable right-handed neutrinos [5, 6]. While the lightest sterile neutrino has tiny couplings to leptons, it can have a significant coupling to an SM singlet S [7]. The latter, in general, mixes with the Higgs field thereby providing us with a channel to probe dark matter via its Higgs couplings. Depending on the coupling strength and the mass, the sterile neutrino may or may not thermalize [8, 9]. If it does, its eventual abundance is determined by the standard freeze-out mechanism, possibly in the relativistic regime [4]. In this work, however, we focus on the non-thermal option.

A popular alternative to the freeze-out dark matter paradigm is provided by the freeze-in mechanism [10], in which case dark matter abundance builds over time without reaching its equilibrium value. Since DM is non-thermal, this mechanism is sensitive to its initial abundance. Although it is common to assume a zero initial value, this assumption is hardly justified in standard cosmological settings due to omnipresent gravitational particle production [11]. In fact, the latter may be responsible for all of the *cold* dark matter in

the form of sterile neutrinos [12]. Their correct abundance can be produced, for example, by the quantum-gravity generated Planck-suppressed operator which couples the sterile neutrinos ν to the inflaton ϕ ,

$$\frac{1}{M_{\text{Pl}}} \bar{\nu}\nu \phi^2 . \quad (1.1)$$

Hence, the gravitational effects are significant and require careful consideration.

The problem of gravitationally produced relics can be addressed by lowering the reheating temperature, which allows for dilution of the former during the inflaton-dominated expansion era [11]. This brings in an interesting possibility that dark matter could be heavier than the SM bath temperature. Its production is then Boltzmann-suppressed such that freeze-in requires larger couplings compared to those in the traditional high- T scenario [13]. As a result, freeze-in dark matter becomes *observable* in direct detection experiments as well as at the LHC.¹ An analogous Boltzmann-suppressed regime in the context of leptogenesis was studied in [15].

In this work, we study the freeze-in mechanism at stronger coupling in the context of sterile neutrino dark matter. Its production by the SM thermal bath is due to the DM coupling to a scalar singlet mixing with the Higgs and is Boltzmann-suppressed. For a broad range of masses above 1 GeV, the sterile neutrino can account for all of the dark matter in the Universe. We consider separately the light and heavy DM regimes, which exhibit different observational signatures, and find exciting prospects for probing freeze-in at stronger coupling.

2 The model

We consider an extension of the SM with a real scalar singlet S and a right-handed Majorana sterile neutrino ν . Although one expects more than one neutrino species to be present, we focus on the lightest one in this work. The relevant part of the neutrino Lagrangian is

$$\mathcal{L} \supset \frac{1}{2} M \bar{\nu}\nu + \frac{1}{2} \lambda S \bar{\nu}\nu + \left(y_{\nu,i} \bar{L}_{L,i} \tilde{H} \nu + \text{h.c.} \right) , \quad (2.1)$$

where \tilde{H} is the charge-conjugate Higgs doublet. We treat the Majorana mass M and the coupling λ as free parameters, while assuming $y_{\nu,i}$ to be negligibly small and irrelevant to our study.²

The scalar potential is taken to be

$$V = \mu_h^2 H^\dagger H + \frac{1}{2} \mu_s^2 S^2 + \lambda_h (H^\dagger H)^2 + \frac{\lambda_s}{4} S^4 + \frac{\lambda_{hs}}{2} S^2 H^\dagger H . \quad (2.2)$$

Although one, in general, expects the terms $SH^\dagger H$ and S^3 to be present, they are not essential for our purposes and we take them to be small.³ We consider the regime where

¹Certain non-trivial high- T freeze-in models, for example, with MeV mediators and millicharged DM, can also have observable signatures [14].

²This can be justified by an approximate Z_2 -parity symmetry $\nu \rightarrow -\nu$.

³They are generated radiatively via the λ -interaction, but can be chosen small at a given scale.

both the Higgs and S develop a non-zero VEV, v_h and v_s , respectively. As a result, these states mix and the mass eigenstates h_1, h_2 are given by

$$\begin{pmatrix} h \\ S \end{pmatrix} = \begin{pmatrix} \cos \theta & \sin \theta \\ -\sin \theta & \cos \theta \end{pmatrix} \begin{pmatrix} h_1 \\ h_2 \end{pmatrix}, \quad (2.3)$$

where θ is the mixing angle,

$$\tan 2\theta = \frac{v_h v_s \lambda_{hs}}{\lambda_s v_s^2 - \lambda_h v_h^2}. \quad (2.4)$$

The state h_1 is identified with the 125 GeV Higgs-like scalar observed at the LHC. In what follows, we treat the mass of the second scalar m_2 along with θ and v_s as input parameters, and present our results in terms of these. The conversion back to the Lagrangian parameters can be implemented with the formulas in [16]. Further discussion of the set-up and related phenomenology can be found in [17].

The sterile neutrino ν plays the role of dark matter. As long as the active-sterile neutrino mixing is tiny, ν is long-lived on cosmological scales (see Fig. 2 of [4]). If its couplings are small, it never thermalizes and can be produced via the freeze-in mechanism. In particular, the scalars h_1 and h_2 remain in thermal equilibrium down to very low temperatures, and source DM production via their couplings to ν . The size of the necessary couplings depends on the temperature of the SM bath T . In what follows, we consider the regime $M \gg T$, in which case the required λ can be as large as $\mathcal{O}(1)$.

3 Boltzmann-suppressed dark matter production

The reheating temperature T_R of the Universe is bounded from below by about 4 MeV [18] and there is no observational evidence that it has ever been high. In fact, dilution of gravitationally produced stable relics favors low reheating temperatures [11]. This is particularly important for freeze-in models, which assume zero initial abundance of dark matter. This assumption is generally violated due to efficient gravitational particle production during and immediately after inflation. The produced particles can however be diluted if the Universe energy density is dominated by a non-relativistic inflaton for a long time, implying a low T_R . In this case, a consistent computation of freeze-in DM production becomes possible [13, 19].

We work under the assumption that the reheating temperature of the Universe does not exceed the electroweak scale. It is then possible that the DM mass scale lies above T_R , in which case dark matter production is Boltzmann-suppressed [13]. More precisely, we assume that M is above the SM bath temperature at any stage of the Universe evolution, i.e. above the maximal temperature (see the discussion in [19]). Dark matter is produced entirely via thermal emission and the exact relic abundance depends on the profile of the temperature evolution. A simple benchmark approximation is obtained by assuming *instant reheating*, i.e. that the SM bath temperature increases abruptly from 0 to T_R . Although this situation is idealized, it gives a good approximation to classes of models with flat temperature profiles before reheating. By rescaling the results, it can be applied to more general situations, as detailed in [19].

The production modes and signatures depend on the DM mass M . For heavy dark matter, it is produced primarily via scattering of the Higgs-like scalars h_1 and h_2 . Light dark matter, on the other hand, is more efficiently produced via SM fermion annihilation. In what follows, we consider these regimes separately.⁴

3.1 Heavy dark matter

This regime is defined by $M^2 \gg m_h^2$. In practise, we take $M > 250$ GeV. Since the bath temperature is far below M , only the most energetic particles from the Boltzmann tail can cause DM production. The main production modes are $h_i h_j \rightarrow \nu\nu$, while the gauge boson fusion is subleading. Unlike Refs. [21, 22], we consider heavy DM such that $h_{1,2}$ decays cannot produce it for kinematic reasons.

Both h_1 and h_2 remain in thermal equilibrium down to very low temperatures. This is due to the efficient reaction $\bar{f}f \leftrightarrow h_{1,2}$, where f is a light SM fermion. It is faster than the expansion of the Universe at temperature T as long as

$$y_{fi} \sqrt{m_{h_i} M_{\text{Pl}}} \gtrsim T, \quad (3.1)$$

omitting unessential factors (below 10). Here y_{fi} ($i = 1, 2$) is the corresponding scalar-fermion Yukawa coupling, $\sqrt{2} \sin \theta m_f / v_h$ or $\sqrt{2} \cos \theta m_f / v_h$. This implies that thermal equilibrium is maintained if $\mathcal{O}(10^{10}) y_{fi} > T / \text{GeV}$, such that for all parameter choices of interest ($\theta \sim 10^{-1}$, $m_2 < \text{TeV}$) both Higgs-like scalars are thermalized.

3.1.1 The Boltzmann equation

The DM number density is determined by the Boltzmann equation. We would like to write it in a convenient form applicable to both pure freeze-in regime, where the sterile neutrinos may not be in kinetic equilibrium with the SM bath, and the regime where DM annihilation becomes tangible and kinetic equilibrium is assumed [23].

Focussing on the Higgs contributions, we have

$$\begin{aligned} \dot{n}_\nu + 3Hn_\nu &= 2\Gamma(h_i h_j \rightarrow \nu\nu) - 2\Gamma(\nu\nu \rightarrow h_i h_j) \\ &= 2\left(\Gamma(h_1 h_1 \rightarrow \nu\nu) + \Gamma(h_1 h_2 \rightarrow \nu\nu) + \Gamma(h_2 h_2 \rightarrow \nu\nu)\right) (1 - n_\nu^2 / n_\nu^{\text{eq}2}), \end{aligned} \quad (3.2)$$

where we have used the Boltzmann distribution for computing the rates⁵ and the second equation assumes kinetic equilibrium. Γ denotes the reaction rate per unit volume. The factor of 2 appears due to particle number change by 2 units in each reaction. In the pure freeze-in regime, the annihilation rate is negligible, i.e. the term proportional to n_ν^2 can be dropped. As the coupling grows, the $h_i - \nu$ system reaches kinetic equilibrium, in which case the production and annihilation rates are related via the chemical potential. At yet larger couplings, the system thermalizes fully and the right hand side vanishes, until DM freeze-out.

⁴We leave out the intermediate mass regime, whose treatment requires more sophisticated numerical tools, e.g. an upgraded version of micrOMEGAs [20].

⁵The quantum statistics effects are very small for particles at the Boltzmann tail.

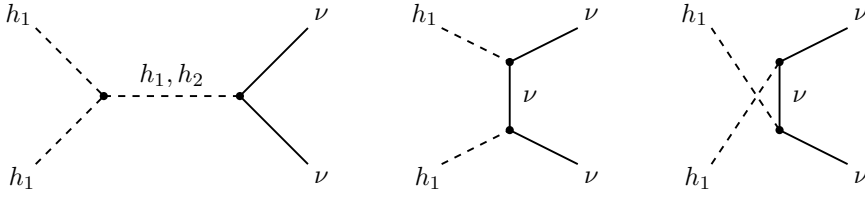


Figure 1: Sterile neutrino production via scalar annihilation $h_1 h_1 \rightarrow \nu \nu$. (Analogous diagrams exist for the $h_2 h_2 \rightarrow \nu \nu$ and $h_1 h_2 \rightarrow \nu \nu$ channels.)

The above Boltzmann equation can be put in a more conventional form using [24]

$$\Gamma(ab \rightarrow cd) = (2\pi)^{-6} \int d^3 p_a d^3 p_b f(p_a) f(p_b) \sigma(p_a, p_b) v_{M\phi l} = n_a n_b \langle \sigma v_{M\phi l} \rangle, \quad (3.3)$$

where f is the momentum distribution function, σ is the reaction cross section which includes the phase space symmetry factors for *both* initial and final particles, $v_{M\phi l}$ is the Møller velocity and $\langle \dots \rangle$ denotes thermal averaging. In kinetic equilibrium, $f = e^{-\frac{E-\mu}{T}}$ with μ being the chemical potential [23, 25]. This, together with energy conservation, implies

$$\Gamma(h_i h_j \rightarrow \nu \nu) = e^{-2\mu/T} \Gamma(\nu \nu \rightarrow h_i h_j) \quad , \quad n_\nu / n_\nu^{\text{eq}} = e^{\mu/T} . \quad (3.4)$$

Then, the Boltzmann equation can be written, for example, in terms of neutrino annihilation cross sections,

$$\dot{n}_\nu + 3H n_\nu = 2 \left(\langle \sigma(\nu \nu \rightarrow h_1 h_1) v \rangle + \langle \sigma(\nu \nu \rightarrow h_1 h_2) v \rangle + \langle \sigma(\nu \nu \rightarrow h_2 h_2) v \rangle \right) \times (n_\nu^{\text{eq}2} - n_\nu^2) . \quad (3.5)$$

The term proportional to $n_\nu^{\text{eq}2}$ is responsible for DM production and valid even in the pure freeze-in regime at feeble couplings. Despite a somewhat deceiving appearance, it *does not* assume that sterile neutrinos are in any kind of equilibrium with the environment. Although the thermal averaging prescription formally requires using the Boltzmann distribution for ν , the full phase space integration makes sure that the resulting $\langle \sigma(\nu \nu \rightarrow h_i h_j) v \rangle n_\nu^{\text{eq}2}$ is just the rate of $h_i h_j \rightarrow \nu \nu$ with thermal h_i, h_j . In contrast, the annihilation term proportional to n_ν^2 assumes chemical potential factorization and, thus, kinetic equilibrium for the $\nu - h_i$ system. This is justified since kinetic equilibrium sets in before DM annihilation becomes important, due to $n_{h_i} \gg n_\nu$.

3.1.2 Relic abundance of dark matter and constraints

The sterile neutrino production processes are shown in Fig. 1. At small λ , the leading contribution comes from the diagrams involving a triple scalar vertex. It is instructive to consider the limit $\theta \ll 1$, in which case the h_2 annihilation via $\Delta\mathcal{L} = \lambda_{222} h_2^3$ dominates and

$$\sigma_{h_2 h_2 \rightarrow \nu \nu} = \frac{1}{2} \times \frac{9 \lambda^2 \lambda_{222}^2}{4\pi s^3} \frac{(s - 4M^2)^{3/2}}{(s - 4m_2^2)^{1/2}} . \quad (3.6)$$

Here we factor out the $1/2$ due to identical particles in the initial state, which is included directly in σ in our convention. s is the Mandelstam variable and $\lambda_{222} \rightarrow \lambda_s v_s$ in the small mixing limit. We observe the velocity suppression v^3 of the result, as expected for production of non-relativistic fermions. The above expression agrees with the result of [8].

The Boltzmann equation can be solved analytically at $M \gg T$ with the above approximations. Using the Gelmini-Gondolo result [24], the rate (3.3) takes the form

$$\Gamma(h_2 h_2 \rightarrow \nu\nu) \simeq \frac{27 \lambda^2 \lambda_{222}^2 T^4}{2^{10} \pi^4 M^2} e^{-2M/T}. \quad (3.7)$$

Here we have used the limit $2M \gg T$ and the corresponding expansion of the Bessel function. Particle production takes place for a short time close to the maximal temperature T_R . Therefore, we may take the number of degrees of freedom g_* approximately constant in this period and the Boltzmann equation in the *pure* freeze-in regime takes the form

$$T^3 \frac{d}{dt} \left(\frac{n_\nu}{T^3} \right) = 2 \Gamma(h_2 h_2 \rightarrow \nu\nu). \quad (3.8)$$

The equation can easily be solved analytically and the resulting DM relic abundance reads

$$Y \equiv \frac{n_\nu}{s_{\text{SM}}} \simeq 1.7 \times 10^{-6} \frac{\lambda^2 \lambda_{222}^2 M_{\text{Pl}}}{M^3} e^{-2M/T_R}, \quad (3.9)$$

where s_{SM} is the Standard Model entropy density, $s_{\text{SM}} = \frac{2\pi^2}{45} g_* T^3$ and $g_* \simeq 107$. The observational constraint $Y = 4.4 \times 10^{-10} \text{ GeV}/M$ then requires

$$\frac{\lambda \lambda_{222}}{M} e^{-M/T_R} \simeq 10^{-11}. \quad (3.10)$$

Therefore, M depends logarithmically on the coupling. Since $M \gg T_R$, order one λ is consistent with freeze-in. For typical $\lambda_{222} \sim \lambda_s v_s$ of order 100 GeV, the neutrino coupling is constrained by $\frac{\lambda}{M/\text{GeV}} e^{-M/T_R} \sim 10^{-13}$. Thus, for $\lambda \sim 1$ and $M \sim 100 \text{ GeV}$, the reheating temperature is about $M/25$.

As the coupling increases, the DM annihilation term becomes important. It reduces the DM density compared to the pure freeze-in approximation and eventually leads to thermalization. In the latter case, $\Gamma(h_i h_j \rightarrow \nu\nu) = \Gamma(\nu\nu \rightarrow h_i h_j)$ until freeze-out, which determines the DM relic abundance. Our full numerical results are presented in Fig. 2. We find that, in the parameter range of interest, the λ_{222} contribution considered above indeed dominates, even at larger λ . The colored lines in the figure correspond to the correct DM relic abundance for a fixed T_R . At sufficiently large coupling, they all merge with the thermal freeze-out curve (black). The latter exhibits a kink at $M = m_2$ due to the annihilation channel $\nu\nu \rightarrow h_2 h_2$ becoming available.

The transition region from pure freeze-in to freeze-out is shown in the right panel of Fig. 2. We see that increasing the coupling beyond a certain limit does not increase the abundance anymore, thermalization sets in and the dependence on T_R is lost. The transition is smooth and shows how the fundamentally different DM regimes are continuously connected, as also observed in Ref. [26].

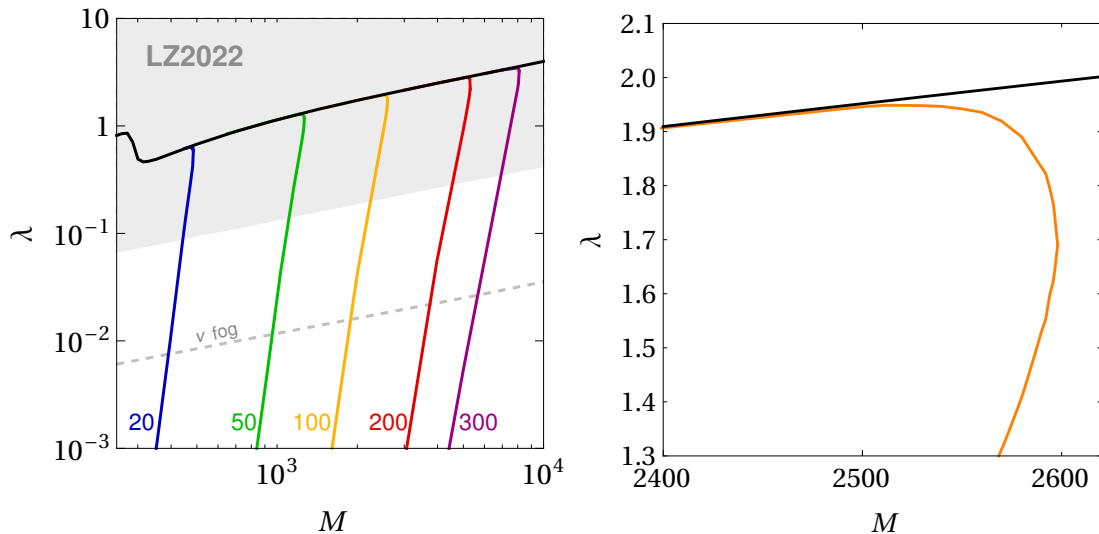


Figure 2: Parameter space for heavy sterile neutrino dark matter with $\sin \theta = 0.2$, $m_2 = 300$ GeV, $v_s = 200$ GeV ($|\lambda_{222}| = 213$ GeV). *Left:* the colored curves correspond to the correct relic abundance for a given T_R in GeV. The black line represents thermal dark matter freeze-out. The shaded area is ruled out by direct DM detection (LZ2022), while the dashed line shows the neutrino background. *Right:* zoomed-in transition region from freeze-in to freeze-out for $T_R = 100$ GeV (yellow line).

The most important constraint on the model is imposed by the direct DM detection bounds [27]. The DM-nucleon scattering cross section is given by

$$\sigma_{\text{SI}} = \frac{\lambda^2 \mu_N^2}{\pi} \left(\frac{f_N m_N}{v_h} \right)^2 \left(\frac{1}{m_1^2} - \frac{1}{m_2^2} \right)^2 \sin^2 \theta \cos^2 \theta, \quad (3.11)$$

where m_N is the nucleon mass, $\mu_N \simeq 1$ GeV is the ν - m_N reduced mass and $f_N \approx 0.3$.

In fermionic dark matter models of the Higgs portal type [28–30], the direct detection constraint (along with the LHC bound) is so strong that it essentially rules out the thermal DM option [31], unless CP violation is allowed [32]. This is mainly due to velocity suppression of DM annihilation, while σ_{SI} is not subject to such suppression. In the case of Boltzmann-suppressed freeze-in, on the other hand, all the constraints are satisfied for couplings below $10^{-1} - 1$ in the mass range $\mathcal{O}(10^2)$ GeV–10 TeV. This parameter space will be continuously probed by current and future direct detection experiments such as XENONnT [33] and DARWIN[34]. Beyond 10 TeV, the sensitivity of these experiments drops, however freeze-in at stronger coupling allows for much higher masses without conflicting perturbativity. Another limitation for the above searches is given by the neutrino background scattering marked by “ ν fog” in the figure.

We have chosen $\sin \theta = 0.2$ and $m_2 = 300$ GeV as a benchmark parameter choice, motivated by the LHC constraints. The LHC searches for a “heavy Higgs” continuously set stricter bounds on the Higgs-like resonances (see e.g. [35]). A recent combination of

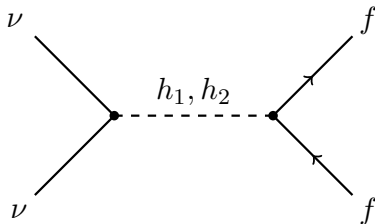


Figure 3: The leading channel for light dark matter production/annihilation ($f = b, c, \tau$).

the LHC constraints on θ, m_2 can be found in [36, 37] and our benchmark represents a reasonable choice.

The scaling of the results with θ and m_2 is readily seen from Eqs. 3.10, 3.11. The relic abundance is independent of θ and m_2 as long as h_2 remains in thermal equilibrium, while it is sensitive to the trilinear coupling λ_{222} . The direct detection constraint is primarily due to the exchange of h_1 , so it is effectively independent of m_2 . On the other hand, it relaxes quickly as θ decreases: the minimal excluded coupling scales as $\lambda \propto 1/\theta$. Therefore, our results for other values of θ and m_2 can be deduced from Fig. 2.

In the above analysis, we have focussed on the DM production via scalar annihilation. The SM fermion annihilation channel is suppressed by the Yukawa couplings and can be neglected. Indeed, although there are many more fermions than the Higgses in the thermal bath, only few of them ($\propto e^{-M/T}$) have enough energy to produce DM. This gives no advantage over the Higgs channel, while there is the Yukawa suppression factor.

3.2 Light dark matter

This regime corresponds to $M \ll m_h$. Since the Boltzmann suppression for DM production is $e^{-M/T}$, it is milder than suppression of the Higgs abundance in the thermal bath $e^{-m_h/T}$ and the Higgs scattering or decay cannot be the leading production channel. The main process is instead $\bar{f}f \rightarrow \nu\nu$, where f is a light SM fermion (Fig. 3).

Analogously to the heavy DM case, the Boltzmann equation can be put in the form

$$\dot{n}_\nu + 3Hn_\nu = 2 \left(\langle \sigma_{\nu\nu \rightarrow b\bar{b}} v \rangle + \langle \sigma_{\nu\nu \rightarrow c\bar{c}} v \rangle + \langle \sigma_{\nu\nu \rightarrow \tau\bar{\tau}} v \rangle \right) \left[(n_\nu^{eq})^2 - n_\nu^2 \right]. \quad (3.12)$$

Here the spin-averaged cross section is

$$\sigma_{\nu\nu \rightarrow f\bar{f}} = \frac{1}{2} \times \frac{N_c y_f^2 \lambda^2}{32\pi s} (s - 4m_f^2)^{3/2} (s - 4M^2)^{1/2} \left[\frac{1}{s - m_1^2} - \frac{1}{s - m_2^2} \right]^2 \sin^2 \theta \cos^2 \theta, \quad (3.13)$$

with $f = b, c, \tau$ and $N_c = 3$ for b and c , and 1 for τ . The Yukawa coupling y_f is defined analogously to that in Eq. 2.1 and the factor of 1/2 is due to identical particles in the initial state, which we include directly in σ . Note that n_ν^{eq} includes 2 spin degrees of freedom.

The analysis proceeds largely parallel to the heavy DM case since the temperature dependence of the reaction rate remains the same, $T^4 e^{-2M/T}$. We take the lowest T_R to be 200 MeV so that the thermal production calculation in terms of elementary fermions is adequate. Below this temperature, the QCD phase transition effects become strong.

The resulting abundance for $m_2^2 \gg m_1^2$ and neglecting the SM fermion mass is

$$Y \simeq \times 10^{-5} N_c y_f^2 \lambda^2 \sin^2 \theta \cos^2 \theta \frac{M^3 M_{\text{Pl}}}{m_1^4} e^{-2M/T_R}. \quad (3.14)$$

Here we have used $g_* \simeq 70$ for temperatures around the GeV, while in general the abundance scales as $g_*^{-3/2}$. When the bottom quark dominates, this sets the constraint

$$\lambda (M/\text{GeV})^2 e^{-M/T_R} \simeq 1.5 \times 10^{-6} / \sin \theta. \quad (3.15)$$

In reality, the fermion masses are not negligible and the RHS of this equation receives the correction factor $(1 - (m_f/M)^2)^{-3/4}$. Order 1 coupling then requires the hierarchy between M and T_R to be somewhat milder than that in the heavy DM case: for typical values $M/T_R \sim 15$.

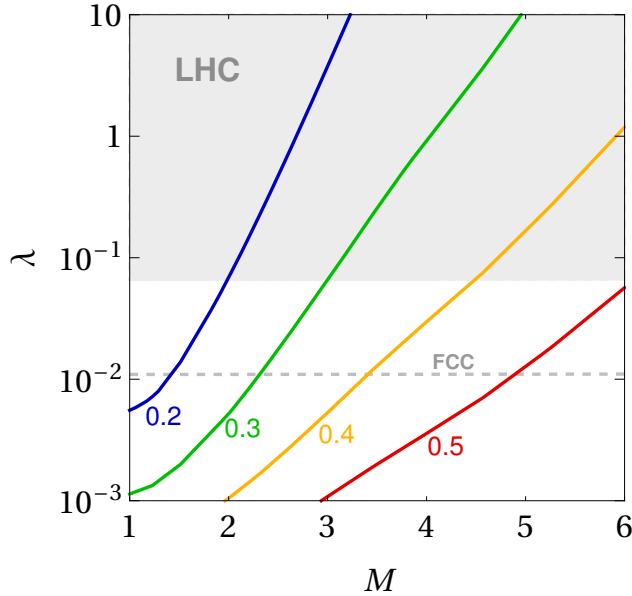


Figure 4: Parameter space for light freeze-in DM at $\sin \theta = 0.2$. The colored curves correspond to the correct relic abundance for a given T_R in GeV. The shaded area is excluded by the LHC measurement of the Higgs invisible decay, while the dashed line shows the FCC prospects in this channel.

For $M < 6$ GeV, the direct DM detection constraints become very loose and the main bound is imposed by the invisible Higgs decay $h_1 \rightarrow \nu\nu$ [31]. The corresponding branching ratio is given by

$$\text{BR}_{\text{inv}} = \frac{\Gamma_{h_1 \rightarrow \nu\nu}}{\cos^2 \theta \Gamma_{\text{SM}}^{\text{tot}} + \Gamma_{h_1 \rightarrow \nu\nu}}, \quad (3.16)$$

where $\Gamma_{\text{SM}}^{\text{tot}}$ is the SM total Higgs width. The decay width into the Majorana sterile neutrinos is

$$\Gamma_{h_1 \rightarrow \nu\nu} = \frac{(m_1^2 - 4M^2)^{3/2}}{16\pi m_1^2} \sin^2 \theta \lambda^2. \quad (3.17)$$

A detailed discussion of the h_1 invisible decay can be found in [38], while for our purposes the above formulae suffice. This observable as a probe of freeze-in was also discussed in [39].

Our results are presented in Fig. 4. We restrict ourselves to the M range between 1 and 6 GeV so that the direct DM detection constraint can be dropped, yet T_R is not too low to avoid complications of the QCD phase transition. The colored curves correspond to the correct DM relic abundance due to freeze-in. The annihilation effect is never important in our parameter range and the thermal abundance would be reached for $\lambda \gg 1$ only, as we have verified numerically. Above the bottom quark threshold, $M > m_b$, b -quark annihilation dominates DM production, while for lower masses, this channel gets suppressed by $e^{-2m_b/T}$ instead of $e^{-2M/T}$. Hence, the c -quark makes the main contribution. Below the charm threshold ($M < 1.3$ GeV), the s -quark dominates and our results become less reliable due to the uncertainty in the s -quark Yukawa coupling. In Fig. 4, we use $m_s \sim 95$ MeV.

We impose the bound of $\text{BR}_{\text{inv}} \lesssim 0.1$ [40] to set the benchmark.⁶ This excludes couplings above 10^{-1} . The HL-LHC will improve the bound on the Higgs coupling strength and BR_{inv} by a factor of a few [41], which allows one to probe the coupling region somewhat below the exclusion line, e.g. by a factor of two. The future collider FCC tuned as a Higgs factory can reach the limit of $\text{BR}_{\text{inv}} \sim 0.003$ (see, e.g. [42]), corresponding to the dashed line in Fig. 4.

Our results shown in Fig. 4 apply to other input parameter choices by a simple rescaling. First, h_2 plays no role at low energies. Second, the combination that enters the observables at $\theta^2 \ll 1$ is $\lambda \sin \theta$. Hence, changing θ amounts to a rescaling λ in this limit.

To conclude, contrary to the thermal dark matter case, there are prospects of observing light non-thermal DM via invisible Higgs decay at both the LHC and FCC. Improvements in its measurement will probe smaller ν couplings in the freeze-in regime.

3.3 Beyond the instant reheating approximation

Our results have been obtained under the simplifying assumption that the SM bath temperature increases from zero to T_R instantaneously. Although this does not appear as a very realistic assumption, our results apply, either directly or via appropriate rescaling, to a broad class of models, where the SM temperature stays constant over cosmological times [19]. In such models, the SM radiation is produced by decay of a field subdominant in the energy balance, instead of the inflaton ϕ . This applies, for example, to the decay cascade $\phi \rightarrow \chi\chi \rightarrow \text{SM}$, where χ is a feebly interacting field. In this case, the temperature of the SM bath remains constant after reaching its maximum, until reheating. DM production occurs most efficiently at the maximal temperature T_{max} , due to the exponential suppression of the rate. When the reheating and maximal temperatures coincide $T_{\text{max}} \simeq T_R$, our results in terms of the (M, λ) parameters apply directly, with a small correction [19].

In general, freeze-in at stronger coupling operates as long as the maximal temperature is well below the DM mass and $T_R < T_{\text{max}}$. The corresponding DM relic abundance Y can

⁶The exact bound depends on the treatment of the Higgs signal strength μ and the ATLAS + CMS result combination.

be obtained by rescaling our results [19]. First, one replaces $T_R \rightarrow T_{\max}$ in the exponent since DM production peaks at that point. Second, one accounts for dilution of DM (entropy production) in the period between T_{\max} and T_R . The latter depends on the scaling of the Hubble rate and T in this period, hence the conclusion is model dependent. The general result is thus

$$Y(T_R) \rightarrow Y(T_{\max}) \times \left(\frac{T_R}{T_{\max}} \right)^\alpha, \quad (3.18)$$

where $Y(T_R)$ represents our result and $\alpha > 0$ is model dependent (see [19] for details). Since the abundance scales as λ^2 , the coupling gets rescaled by the square root of the above factor. The result is therefore model-dependent, which is inherent in any non-thermal DM model. For example, the conventional high- T freeze-in models suffer from the uncontrollable gravitational particle production background [11].

Generally, there is no evidence in favor of a specific mechanism of the SM particle generation or a particular range of T_R . In this work, we take an agnostic stance on this matter and treat DM production from the effective low energy perspective. Our assumptions are that the initial DM abundance is negligible and that DM is primarily produced by the SM thermal bath. These may or may not be realistic in a given UV complete framework.

4 Conclusion

Freeze-in at stronger coupling occurs when the dark matter mass exceeds the Standard Model bath temperature. The dark matter coupling is allowed to be as large as order one, without thermalizing the system. At yet larger couplings, dark matter equilibrates with the SM thermal bath and one recovers the usual DM freeze-out. In this sense, the regime of freeze-in at stronger coupling interpolates between freeze-in and freeze-out.

In this work, we have studied sterile neutrino DM freeze-in at stronger coupling. It couples to a singlet scalar, which mixes with the Higgs and thus allows for thermal production of sterile neutrinos. Although the usual DM freeze-out is ruled by the direct detection constraints, freeze-in at stronger coupling is consistent with the bounds and can account for the observed (cold) DM density. The scenario is currently being probed by the direct detection experiments and, as their sensitivity improves down to the “neutrino floor”, lower couplings and higher reheating temperatures will be continuously explored. For light (GeV scale) dark matter, the main signature is provided by the invisible Higgs decay at the LHC. Part of the parameter space is already excluded, while lower couplings corresponding to the Higgs BR_{inv} at the percent level and below will be probed at the HL-LHC and the FCC.

We note that the scenario considered is well theoretically motivated. Indeed, the usual freeze-in models suffer from the problem of initial conditions: gravitational inflationary and postinflationary particle production creates a strong background for the abundance calculations. The problem can be addressed by lowering the reheating temperature, in which case the dark matter mass scale could readily exceed the SM bath temperature. Then, freeze-in at stronger coupling would be the leading mechanism for DM production.

Acknowledgements. OL is grateful to Tania Robens for useful communications. This work was supported by the Estonian Research Council grants PRG803, PRG1677, RVTT3, RVTT7, and the CoE program TK202 “Fundamental Universe”.

A Appendix

In this Appendix, we list some of the analytical results for the cross sections we use in our study. The thermal averaged cross section for the process $h_i h_j \rightarrow \nu\nu$ reads

$$\langle \sigma_{h_i h_j \rightarrow \nu\nu} \rangle = \frac{1}{n_{h_i}^{eq} n_{h_j}^{eq}} \frac{T}{32\pi^4} \int_{4M^2}^{\infty} ds [s - (m_i + m_j)^2] [s - (m_i - m_j)^2] \frac{\sigma_{h_i h_j \rightarrow \nu\nu}}{\sqrt{s}} K_1(\sqrt{s}/T). \quad (\text{A.1})$$

Defining the scalar trilinear couplings as

$$\mathcal{L}_{ijk} = \lambda_{ijk} h_i h_j h_k, \quad (\text{A.2})$$

we find the following production cross sections (including the *initial* state phase space symmetry factors):

$$\sigma_{h_1 h_1 \rightarrow \nu\nu} = \frac{1}{128\pi s} \frac{\sqrt{s - 4M^2}}{\sqrt{s - 4m_1^2}} \left[A_{11} + B_{11} \log \left(\frac{s - 2m_1^2 + \sqrt{s - 4m_1^2} \sqrt{s - 4M^2}}{s - 2m_1^2 - \sqrt{s - 4m_1^2} \sqrt{s - 4M^2}} \right) \right], \quad (\text{A.3})$$

where

$$\begin{aligned} A_{11} &= 4(s - 4M^2) \left(\frac{(-\sin \theta\lambda)(3! \lambda_{111})}{s - m_1^2} + \frac{(\cos \theta\lambda)(2! \lambda_{112})}{s - m_2^2} \right)^2 \\ &\quad - 32M(-\sin \theta\lambda)^2 \left(\frac{(-\sin \theta\lambda)(3! \lambda_{111})}{s - m_1^2} + \frac{(\cos \theta\lambda)(2! \lambda_{112})}{s - m_2^2} \right) \\ &\quad - \frac{8(-\sin \theta\lambda)^4(2sM^2 + 16M^4 - 16M^2m_1^2 + 3m_1^4)}{sM^2 - 4M^2m_1^2 + m_1^4}, \\ B_{11} &= -\frac{16M(-\sin \theta\lambda)^2(s - 8M^2 + 2m_1^2)}{\sqrt{s - 4m_1^2} \sqrt{s - 4M^2}} \left(\frac{(-\sin \theta\lambda)(3! \lambda_{111})}{s - m_1^2} + \frac{(\cos \theta\lambda)(2! \lambda_{112})}{s - m_2^2} \right) \\ &\quad + \frac{8(-\sin \theta\lambda)^4(s^2 + 16sM^2 - 32M^4 + 6m_1^4 - 4sm_1^2 - 16M^2m_1^2)}{(s - 2m_1^2)\sqrt{s - 4m_1^2} \sqrt{s - 4M^2}}, \end{aligned} \quad (\text{A.4})$$

$$\sigma_{h_2 h_2 \rightarrow \nu\nu} = \frac{1}{128\pi s} \frac{\sqrt{s - 4M^2}}{\sqrt{s - 4m_2^2}} \left[A_{22} + B_{22} \log \left(\frac{s - 2m_2^2 + \sqrt{s - 4m_2^2} \sqrt{s - 4M^2}}{s - 2m_2^2 - \sqrt{s - 4m_2^2} \sqrt{s - 4M^2}} \right) \right], \quad (\text{A.6})$$

where

$$\begin{aligned} A_{22} &= 4(s - 4M^2) \left(\frac{(-\sin \theta\lambda)(2! \lambda_{221})}{s - m_1^2} + \frac{(\cos \theta\lambda)(3! \lambda_{222})}{s - m_2^2} \right)^2 \\ &\quad - 32M(\cos \theta\lambda)^2 \left(\frac{(-\sin \theta\lambda)(2! \lambda_{221})}{s - m_1^2} + \frac{(\cos \theta\lambda)(3! \lambda_{222})}{s - m_2^2} \right) \\ &\quad - \frac{8(\cos \theta\lambda)^4(2sM^2 + 16M^4 - 16M^2m_2^2 + 3m_2^4)}{sM^2 - 4M^2m_2^2 + m_2^4}, \end{aligned} \quad (\text{A.7})$$

$$B_{22} = -\frac{16M(\cos\theta\lambda)^2(s-8M^2+2m_2^2)}{\sqrt{s-4m_2^2}\sqrt{s-4M^2}} \left(\frac{(-\sin\theta\lambda)(2!\lambda_{221})}{s-m_1^2} + \frac{(\cos\theta\lambda)(3!\lambda_{222})}{s-m_2^2} \right) + \frac{8(\cos\theta\lambda)^4(s^2+16sM^2-32M^4+6m_2^4-4sm_2^2-16M^2m_2^2)}{(s-2m_2^2)\sqrt{s-4m_2^2}\sqrt{s-4M^2}}, \quad (\text{A.8})$$

$$\sigma_{h_1 h_2 \rightarrow \nu\nu} = \frac{1}{64\pi s} \frac{\sqrt{s-4M^2}}{\sqrt{s-2(m_1^2+m_2^2)} + (m_1^2-m_2^2)^2/s} \left[A_{12} + B_{12} \log \left(\frac{s-m_1^2-m_2^2 + \sqrt{s-4M^2}\sqrt{s-2(m_1^2+m_2^2)} + (m_1^2-m_2^2)^2/s}{s-m_1^2-m_2^2 - \sqrt{s-4M^2}\sqrt{s-2(m_1^2+m_2^2)} + (m_1^2-m_2^2)^2/s} \right) \right], \quad (\text{A.9})$$

where

$$A_{12} = 4(s-4M^2) \left(\frac{(-\sin\theta\lambda)(2!\lambda_{112})}{s-m_1^2} + \frac{(\cos\theta\lambda)(2!\lambda_{221})}{s-m_2^2} \right)^2 - 32M(-\sin\theta\lambda)(\cos\theta\lambda) \left(\frac{(-\sin\theta\lambda)(2!\lambda_{112})}{s-m_1^2} + \frac{(\cos\theta\lambda)(2!\lambda_{221})}{s-m_2^2} \right) - \frac{8(-\sin\theta\lambda)^2(\cos\theta\lambda)^2[2sM^2+16M^4-8M^2(m_1^2+m_2^2)+3m_1^2m_2^2-2M^2(m_1^2-m_2^2)/s]}{sM^2-2M^2(m_1^2+m_2^2)+m_1^2m_2^2+M^2(m_1^2-m_2^2)^2/s}, \quad (\text{A.10})$$

$$B_{12} = -\frac{16M(-\sin\theta\lambda)(\cos\theta\lambda)(s-8M^2+m_1^2+m_2^2)}{\sqrt{s-4M^2}\sqrt{s-2(m_1^2+m_2^2)} + (m_1^2-m_2^2)^2/s} \left(\frac{(-\sin\theta\lambda)(2!\lambda_{112})}{s-m_1^2} + \frac{(\cos\theta\lambda)(2!\lambda_{221})}{s-m_2^2} \right) + \frac{8(-\sin\theta\lambda)^2(\cos\theta\lambda)^2[s^2+16sM^2-32M^4+m_1^4+4m_1^2m_2^2+m_2^4-2s(m_1^2+m_2^2)-8M^2(m_1^2+m_2^2)]}{(s-m_1^2-m_2^2)\sqrt{s-4M^2}\sqrt{s-2(m_1^2+m_2^2)} + (m_1^2-m_2^2)^2/s}.$$

References

- [1] S. Dodelson and L. M. Widrow, Phys. Rev. Lett. **72**, 17 (1994).
- [2] X. D. Shi and G. M. Fuller, Phys. Rev. Lett. **82**, 2832 (1999).
- [3] A. Boyarsky, M. Drewes, T. Lasserre, S. Mertens and O. Ruchayskiy, Prog. Part. Nucl. Phys. **104**, 1-45 (2019).
- [4] O. Lebedev and T. Toma, JHEP **05**, 108 (2023).
- [5] T. Asaka, S. Blanchet and M. Shaposhnikov, Phys. Lett. B **631**, 151 (2005).
- [6] T. Asaka, M. Laine and M. Shaposhnikov, JHEP **0701**, 091 (2007); Erratum: [JHEP **1502**, 028 (2015)].
- [7] A. Kusenko, Phys. Rev. Lett. **97**, 241301 (2006).
- [8] V. De Romeri, D. Karamitros, O. Lebedev and T. Toma, JHEP **10**, 137 (2020).
- [9] R. Coy and M. A. Schmidt, JCAP **08**, 070 (2022).
- [10] L. J. Hall, K. Jedamzik, J. March-Russell and S. M. West, JHEP **03**, 080 (2010).
- [11] O. Lebedev, JCAP **02**, 032 (2023).

- [12] F. Koutroulis, O. Lebedev and S. Pokorski, “Gravitational production of sterile neutrinos,” [arXiv:2310.15906 [hep-ph]], *to appear in JHEP*.
- [13] C. Cosme, F. Costa and O. Lebedev, “Freeze-in at stronger coupling,” [arXiv:2306.13061 [hep-ph]], *to appear in Phys. Rev. D*.
- [14] T. Hambye, M. H. G. Tytgat, J. Vandecasteele and L. Vanderheyden, *Phys. Rev. D* **98**, no.7, 075017 (2018).
- [15] G. F. Giudice, A. Notari, M. Raidal, A. Riotto and A. Strumia, *Nucl. Phys. B* **685**, 89-149 (2004).
- [16] A. Falkowski, C. Gross and O. Lebedev, *JHEP* **05**, 057 (2015).
- [17] O. Lebedev, *Prog. Part. Nucl. Phys.* **120**, 103881 (2021).
- [18] S. Hannestad, *Phys. Rev. D* **70**, 043506 (2004).
- [19] C. Cosme, F. Costa and O. Lebedev, “Temperature evolution in the Early Universe and freeze-in at stronger coupling,” [arXiv:2402.04743 [hep-ph]].
- [20] G. Belanger, F. Boudjema and A. Pukhov, “micrOMEGAs : a code for the calculation of Dark Matter properties in generic models of particle interaction,” [arXiv:1402.0787 [hep-ph]].
- [21] M. Drewes and J. U. Kang, *JHEP* **05**, 051 (2016).
- [22] J. König, A. Merle and M. Totzauer, *JCAP* **11**, 038 (2016).
- [23] E. W. Kolb and M. S. Turner, *Front. Phys.* **69**, 1-547 (1990).
- [24] P. Gondolo and G. Gelmini, *Nucl. Phys. B* **360**, 145-179 (1991).
- [25] J. Bernstein, L. S. Brown and G. Feinberg, *Phys. Rev. D* **32**, 3261 (1985).
- [26] J. Silva-Malpartida, N. Bernal, J. Jones-Pérez and R. A. Lineros, *JCAP* **09**, 015 (2023).
- [27] J. Aalbers *et al.* [LZ], *Phys. Rev. Lett.* **131**, no.4, 041002 (2023).
- [28] Y. G. Kim and K. Y. Lee, *Phys. Rev. D* **75**, 115012 (2007).
- [29] Y. G. Kim, K. Y. Lee and S. Shin, *JHEP* **05**, 100 (2008).
- [30] S. Baek, P. Ko and W. I. Park, *JHEP* **02**, 047 (2012).
- [31] A. Djouadi, O. Lebedev, Y. Mambrini and J. Quevillon, *Phys. Lett. B* **709**, 65-69 (2012).
- [32] L. Lopez-Honorez, T. Schwetz and J. Zupan, *Phys. Lett. B* **716**, 179-185 (2012).
- [33] E. Aprile *et al.* [XENON], *JCAP* **11**, 031 (2020).
- [34] J. Aalbers *et al.* [DARWIN], *JCAP* **11**, 017 (2016).
- [35] G. Aad *et al.* [ATLAS], *JHEP* **07**, 200 (2023).
- [36] T. Robens, *Springer Proc. Phys.* **292**, 141-152 (2023) [arXiv:2209.15544 [hep-ph]].
- [37] Tania Robens, *private communication*.
- [38] T. Biekötter and M. Pierre, *Eur. Phys. J. C* **82**, no.11, 1026 (2022).
- [39] T. Bringmann, S. Heeba, F. Kahlhoefer and K. Vangsnes, *JHEP* **02**, 110 (2022).
- [40] [ATLAS], “Combination of searches for invisible Higgs boson decays with the ATLAS experiment,” ATLAS-CONF-2020-052.

- [41] P. A. Rivadeneira Bracho, “Search for invisible decays of the Higgs boson produced via vector boson fusion at the ATLAS detector with 139 fb⁻¹ of integrated luminosity,” *PhD thesis, University of Hamburg, 2022*.
- [42] P. Giacomelli, *talk at ICHEP 2018*,
https://indico.cern.ch/event/686555/contributions/2971566/attachments/1682031/2703684/Higgs-measurements-FCC-ICHEP-2018_169.pdf